2D Black Phosphorus/$SrTiO_3$-Based Programmable Photoconductive Switch

Fucai Liu, Chao Zhu, Lu You, Shi-Jun Liang, Shoujun Zheng, Jiadong Zhou, Qundong Fu, Yongmin He, Qingsheng Zeng, Hong Jin Fan, Lay Kee Ang, Junling Wang, and Zheng Liu**

Heterostructures on the nanometer scale have led to completely new physical behaviors and functionalities. Oxides and 2D materials are two excellent but isolated platforms for the creation of functional heterostructures. The quasi-free-standing nature of 2D materials allows the realization of heterostructure by stacking different 2D crystals on top of each other in a precise sequence, which is often referred to as van der Waals (vdW) heterostructure.[1–7] While the ultrasensitivity of structural distortions and crystal chemistry from various transition-metal oxide materials[8] result into a number of novel phenomena at complex oxide interfaces, such as the ferromagnetic metallic states in superlattice composed of antiferromagnetic insulators,[9] the superconductivity and ferromagnetism at interface between two dielectrics,[10,11] and the enhanced critical temperatures in high T_c superconductor heterostructures.[12] The marriage of 2D materials and oxides may provide a scaffold for a large varies of unprecedented heterostructures and novel devices.

Dr. F. Liu, C. Zhu, J. Zhou, Q. Fu, Dr. Y. He, Dr. Q. Zeng, Prof. Z. Liu
Centre for Programmable Materials
School of Materials Science and Engineering
Nanyang Technological University
50 Nanyang Avenue, Singapore 639798, Singapore
E-mail: fucailiu@gmail.com; z.liu@ntu.edu.sg
Dr. L. You, Prof. J. Wang
School of Materials Science and Engineering
Nanyang Technological University
50 Nanyang Avenue, Singapore 639798, Singapore
S. Liang, Prof. L. K. Ang
Engineering Product Development
Singapore University of Technology and Design
8 Somapah Road, Singapore 487372, Singapore
S. Zheng, Prof. H. J. Fan
Centre for Disruptive Photonic Technologies
School of Physics and Mathematics Sciences
Nanyang Technological University
21 Nanyang Link, Singapore 637371, Singapore
Prof. Z. Liu
Centre for Micro/Nano-electronics (NOVITAS)
School of Electrical and Electronic Engineering
Nanyang Technological University
50 Nanyang Avenue, Singapore 639798, Singapore
Prof. Z. Liu
CINTRA CNRS/NUT/THALES, UMI 3288
Research Techno Plaze
50 Nanyang Drive, Border X Block, Level 6
Singapore 637553, Singapore

DOI: 10.1002/adma.201602280

Among the transition-metal oxides, one of the most important and widely used constituent materials is strontium titanate ($SrTiO_3$, STO). Based on it, a great number of complex oxide structures were built and numerous interesting phenomena have been reported. For example, lanthanum aluminate/strontium titanate ($LaAlO_3/SrTiO_3$) interfaces exhibit metallic conductivity,[13] superconductivity and ferromagnetism,[10,11] which are not found in the constituent materials. Single-layer FeSe grown on STO shows superconductivity with T_c above 100 K.[14] Light-induced gating effect or magnetization have also been discovered in the STO or related heterostructures.[15–17]

On the other hand, unusual properties and new phenomena have been revealed in 2D van der Waals solids (vertical heterostructures). Exceptionally high mobility has been observed in the graphene/BN heterostructure.[18] Light–matter interaction has been greatly enhanced in semiconducting transition-metal dichalcogenides (TMDs)/graphene heterostructure, leading to enhanced photon absorption and electron–hole generation.[19] Light-emitting diodes fabricated by vertically stacked graphene, hexagonal boron nitride, and various semiconducting TMD monolayers have exhibited an extrinsic quantum efficiency of nearly 10%.[20] Ultrafast photoresponse and long lived interlayer exciton have also been observed in the vdW heterostructure.[21–23] Stacking the functional 2D materials with strongly correlated oxide substrate will open new avenues for heterostructure fabrication, unique properties and novel phenomena are also highly expected, as evidenced by the pioneer work of high temperature superconductivity in FeSe/STO heterostructure.[14] Here, we report a new strategy to fabricate heterostructure based on BP, a unique 2D material with high mobility and in-plane anisotropy, and STO, a widely used oxide substrate. In contrast to the BP device fabricated on SiO_2 substrate, remarkable optoelectronic functionalities of the light-tunable persistent photoconductivity with large on/off ratio exceeding 10^5 was observed in the BP/STO heterostructure.

Similar to graphite and transition-metal dichalcogenides (TMDs), black phosphorus (BP) is a layered crystal and has recently been rediscovered from the perspective of 2D material.[24–27] It has shown excellent electrical properties, including a high hole mobility up to 1000 $cm^2\ V^{-1}\ s^{-1}$,[24] an on/off ratio up to 10^5, with excellent transport properties,[28–30] has regained remarkable interests for potential applications in high-performance thin-film electronics. Moreover, bulk BP has a bandgap of ≈0.3 eV. As the number of layer decreases, the bandgap increases and eventually reaches to 1.8–2.0 eV in the monolayer.[31,32] Such a layer-dependent bandgap covering the visible to mid-infrared spectral range suggests that BP is

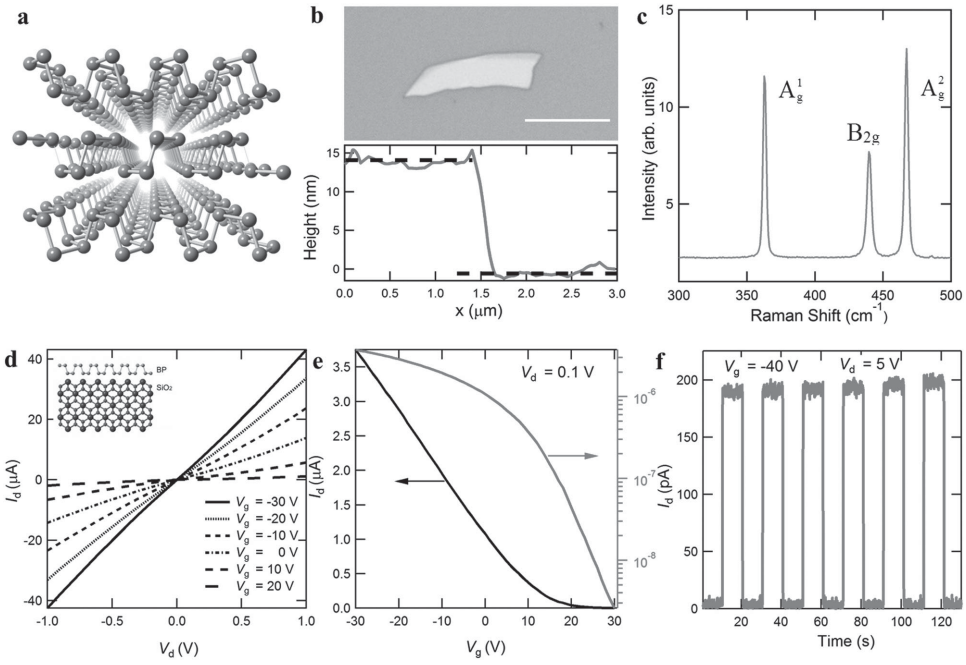

Figure 1. Characterization of the BP FET device and photoresponse on SiO_2 substrate. a) Crystal structure of BP. b) Typical optical image (top) and height profile (bottom) of the BP thin flake on SiO_2 substrate. Scale bar, 10 μm. c) Raman spectrum of BP thin flake. d) The typical output and (e) transfer curve of BP FET on SiO_2 substrate. Inset of (d) shows the schematic of BP/SiO_2 heterostructure. f) Time-dependent photocurrent change of BP transistor on SiO_2 substrate measured at room temperature, with a gate voltage of −40 V and drain voltage of 5 V.

a very promising 2D material for broadband optoelectronic applications.[33–35] Due to the large tunable bandgap, BP has also been used as a broadband absorber from visible to mid-infrared range.[36] With its puckered orthorhombic structure of the D_{2h} point group (**Figure 1**a), the effective mass of carriers of BP along the zigzag direction is about 10 times larger than that along the armchair direction, which induces strong in-plane anisotropy of its electronic, optical, and phonon properties.[25,37–39] Such properties may enable a new domain of electronic and photonic device research where the strong anisotropic properties of 2D materials could be used to design new electronic and optoelectronic devices.

Before investigating the BP/STO heterostructure, we first exfoliate the BP thin flakes on the Si substrates covered with 285 nm SiO_2, and measure the intrinsic field effect mobility and photoresponsivity. A typical optical image and height profile of the BP flake are shown in Figure 1b. The Raman scattering spectra have used to identify the crystalline orientation of BP flakes as well as the layer number.[40] Figure 1c shows Raman spectra of BP. We observe three Raman peaks in BP thin flake at around 470, 440, and 365 cm^{-1}, corresponding to the A_g^2, B_{2g}, and A_g^1 modes, respectively, which agree well with previous observations in few-layer BP flakes.[41] These sharp modes correspond to the unique orthorhombic crystalline phosphorus structure (Figure S2, Supporting Information). In addition, TEM characterization (see Figure S1, Supporting Information) also confirms the highly crystalline structure of BP.

BP field-effect transistor is fabricated through photolithography on Si/SiO_2 substrate. We perform electrical characterizations of our devices in a vacuum chamber at room temperature, the transfer and output curves are shown in Figure 1d,e, respectively. The nearly linear I_d–V_d curve at low voltage indicates the low Schottky barrier at the metal/BP interface. The transfer curve reveals a p-type behavior of the BP devices. By fitting the I_d–V_g curve in the V_g from −10 V to −30 V, the mobility of the channel is deduced to be 149 cm^2 V^{-1} s^{-1}, calculated by using the equation $\mu = dI_d/dV_g \times (L/WC_iV_d)$, where L is channel length (4.5 μm), W is the channel width (9 μm), and C_i is the capacitance between the channel and the back gate per unit area ($C_i = \varepsilon_0\varepsilon_r/d$.: ε_0 is vacuum permittivity, ε_r is the relative permittivity, and d is the thickness of SiO_2 layer of 285 nm). The calculated mobility is comparable with other reported value.[24,27] Due to the semiconducting nature of BP, the transistor shows an on/off ratio of around 10^5. We then evaluate the photoresponse of the fabricated BP FETs. The measurements are carried out by mechanically modulating the intensity of the incoming light (633 nm) and recording the current under constant V_d = 5 V and −40 V gate bias. Figure 1f shows the measured photocurrent with a light power of 2 mW, which is in phase with the excitation modulation. The photoresponsivity R, calculated by $R = I_{ph}/P$ (I_{ph} is generated photocurrent, P is the light power absorbed by the device channel), is around 2.5 A W^{-1}, higher than the reported value of 0.66 A W^{-1}.[34] This might be due to the difference of the applied gate voltage and drain voltage, which can tune the Schottky barrier height and electron–hole separation rate for the photocurrent generation, respectively.

In contrast to the SiO_2 substrate, STO dramatically change the behavior of the device due to strong interaction between the layers. Details of the device fabrication are shown in the method part (Figure S3, Supporting Information). The photoresponse properties of the heterostructure device were carried out

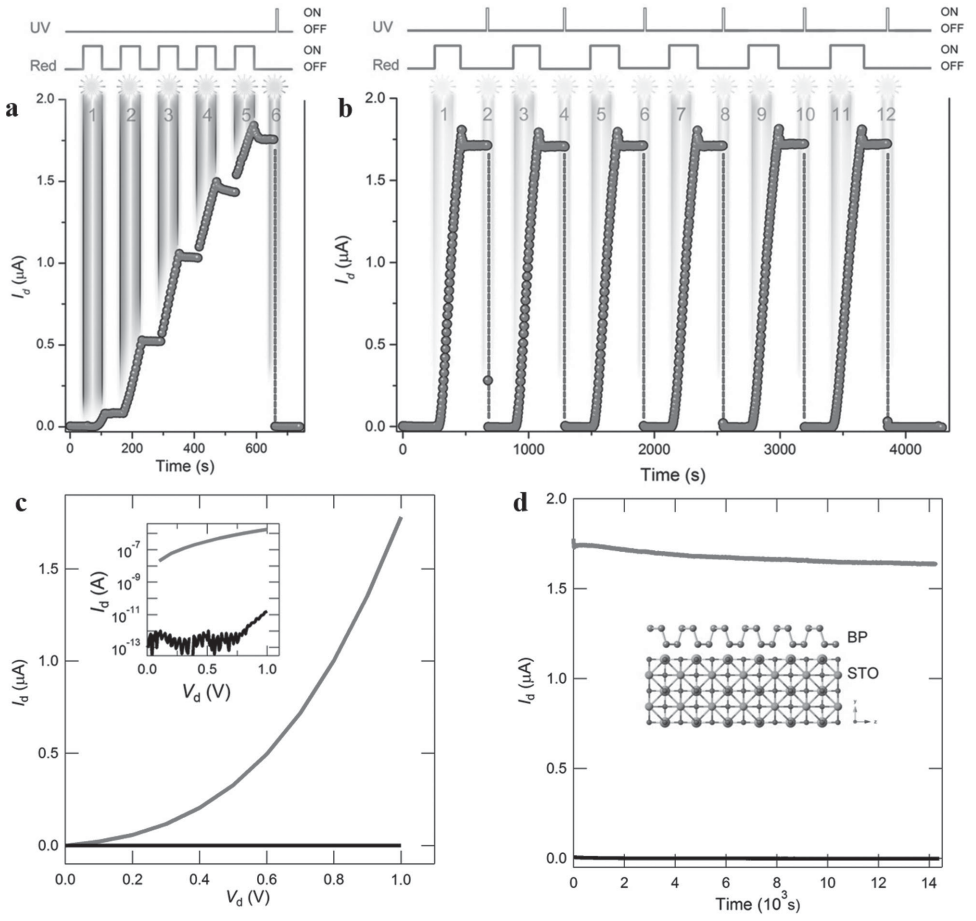

Figure 2. Photoresponse and persistent photocurrent of BP/STO device at 50 K. a) The photocurrent change with only red light is switched on and off alternatively at 50 K. Red light induced a persistent photocurrent and it does not saturate after a few times illumination. The current remains even the light is off. UV light will reset the current close to zero in a short time (≈2 s). b) The photocurrent change with both red and UV is switched on and off alternatively at 50 K. c) The I_d–V_d curve of the device under the on and off state indicated in (b). Inset shows the plot in semi-log scale. d) Nearly relaxation-free nature of persistent photocurrent at on and off states, respectively. Inset shows the schematic of BP/$SrTiO_3$ heterostructure.

at low temperature (50 K). As can be seen in **Figure 2**a, the current increases step by step with switching on and off the red light illumination, which is in contrast with the photoresponse behavior of BP device on SiO_2. Even though a high photocurrent is obtained, 2 s illumination of UV light makes current drop dramatically. Figure 2b shows the time-dependent photocurrent of the device with a few cycles of alternative red and UV light illumination. The photocurrent periodically increases and decreases upon the light-on and light-off conditions at a 1 V bias voltage, respectively, indicating excellent response and reliability of the device. Figure 2c shows the I_d–V_d curves under ON and OFF states at 50 K. The current on/off ratio of the device were achieved to ≈10^5, significantly higher than that of the reported photodetection device based on other 2D materials like graphene,[42] TMDs,[43] and a few order of magnitudes higher than pristine BP,[35] which is also larger than the hybrid device based on graphene/MoS_2.[44] By subtracting the OFF current from the ON current, the responsivity of light-induced current change is calculated to be 1.1×10^5 A W^{-1}, which is about 10^5 times larger than that of the photoresponse for the BP phototransistor integrated with waveguide,[34] and comparable with the recent reported value based on BP device with narrow channel length (but with very low on/off ratio).[45] In addition to the high photosensitivity of the heterostructure device, the current can keep a long time. As shown in Figure 2d, the current almost keeps constant for more than 4 h. A decay time of several days can be deduced by fitting the experimental data. We also compared the room temperature photoresponse of BP/STO heterostructure with BP device on SiO_2 substrate. Significant different behavior is also observed even at room temperature (see Figure S4, Supporting Information). Similar persistent photocurrent behavior is also observed in MoS_2/STO heterostructure (Figure S6, Supporting Information).

To understand the tremendously enhanced responsivity as well as persistent photocurrent in the heterostructure device, we perform the wavelength-dependent photoresponse measurement. As can be seen in **Figure 3**a–c, under the fixed illumination light intensity, the photocurrents induced by the illumination of 633, 532, and 405 nm are ≈1.8 μA, 120 nA and 25 nA, respectively, indicating that wavelength plays an important role in the enhancement of responsivity and persistent photoconductivity. These phenomena can be explained by a model based on electron-hole generation and recombination process related to optical absorption and defects in STO.[17]

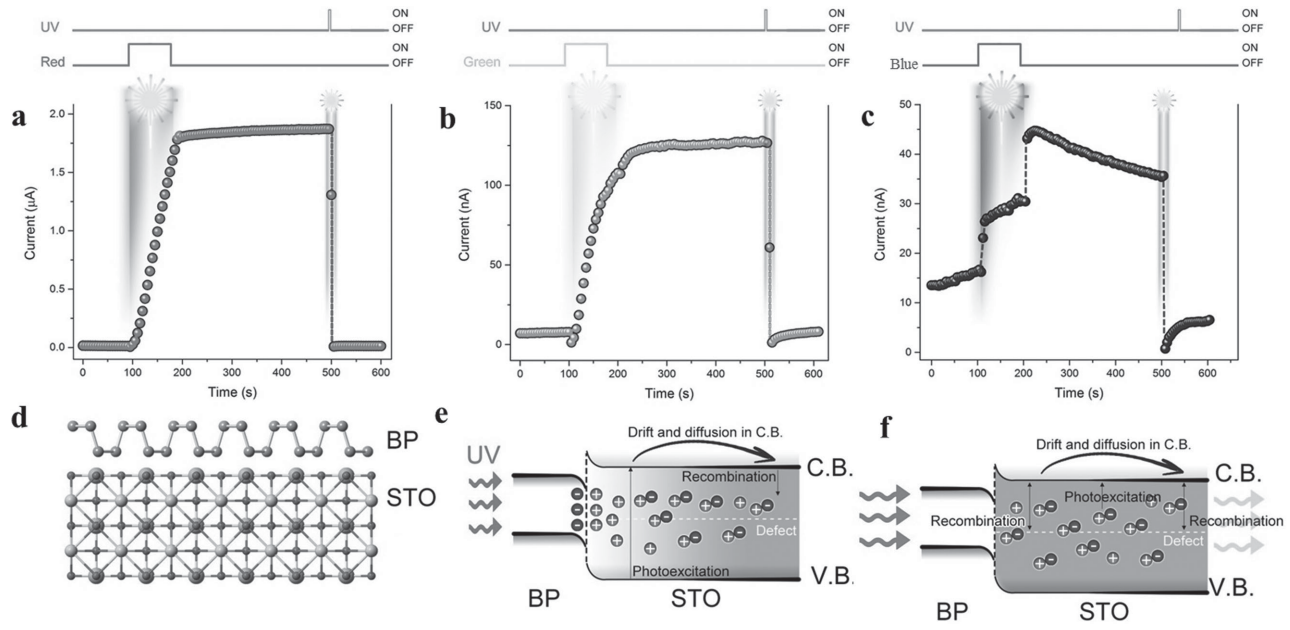

Figure 3. Light-wavelength-dependent photoresponse of BP/STO device. The photocurrent evaluation under the illumination of (a) red, (b) green, and (c) blue light illumination at 50 K. d) Schematic of the BP/STO heterostructure. e,f) The photocarriers' generation, transport, and recombination dynamics under (e) UV and (f) red light illumination, respectively.

Generally, there are numerous donor and acceptor states generated by intrinsic defects in STO.[46,47] Due to the variation in absorption, the optical penetration depth and excited energy state of different state changes accordingly depending on the wavelength of the incident light. For example, UV light can excite both the deep and low defect levels but within very limited thickness below the surface (Figure 3e). While red light could penetrate through the entire sample, and excite the low defect levels (see transmission spectrum of STO in Figure S5, Supporting Information). Under light illumination, the semiconductor heterostructure undergoes various electron–hole pairs generation, diffusion, and recombination process. The UV light only generates electron–hole pairs close the surface layer. If the generated electrons diffused to the deep inside layer and recombines with the acceptor centers there, they will be unlikely to be re-excited and remains there even after the light is switched off (Figure 3e). This results in a built-in electric field at the interface of BP and STO due to the accumulation of holes at the surface of BP. As a consequence, electrons are accumulated in the BP layer, reducing the photoconductivity of BP due to its p-type nature. In contrast, red light can excite the frozen electrons from the acceptor states located in the deep layer, which recombines with holes at top layer (Figure 3f). Meanwhile, the built-in electric field is cancelled, and photoconductivity of BP layer increases. This light-tunable effect at the BP/STO interface enables a high responsivity and persistent photoconductivity in black phosphorus.

To further explore the optical gating induced persistent photocurrent, we examine the temperature dependence of photoresponse from room temperature down to 50 K. The time-dependent response of the three processes are studied: (I) the current rising process under the illumination of red light, (II) the current decaying process just after the red light is off (ON state), (III) the current decay process after the UV light is off (OFF state). The normalized time resolved current change of each process is shown in the Figure S7–S9 (Supporting Information). The time constant at various temperatures is obtained via fitting and they are plotted in **Figure 4**. When shed the red light on device, the relaxation time is mainly determined by the trap level. Therefore, we fit experimental data (sphere symbol) by using $\tau_0 e\frac{T_0}{T}$, and both are in excellent agreement. When red light is off, the relaxation process can be attributed to scattering, which gives $\tau \propto T^{3/2}$. Using this scaling to fit red decay time (solid sphere) gives a good agreement. For UV decay time, we use a combination of exponential function and power law to account for the combined effects from defects scattering and trap excitation.

In conclusion, we have observed the giant photoresponsivity in BP/STO heterostructure. The responsivity of light-induced current change exceeds 10^5 A W^{-1}. Also, persistent photocurrent effect is observed at low temperature, where the photocurrent is not relaxed after the light is switched off. The on/off ratio achieves 10^5. The experimental results can be accounted by the optical gating effect at the interface of BP/STO, which is consistent with the theoretical model based on the charge transfer under light illumination. This work opens the door to new type of heterostructures consisting of 2D material and oxides, and will pave a way to novel optoelectronic and memory devices.

Experimental Section

Characterization of BP Thin Flakes Transistor: First the BP flakes were obtained by means of mechanically exfoliation of bulk single crystal on the Si or $SrTiO_3$ substrates, and identified by optical microscopy.

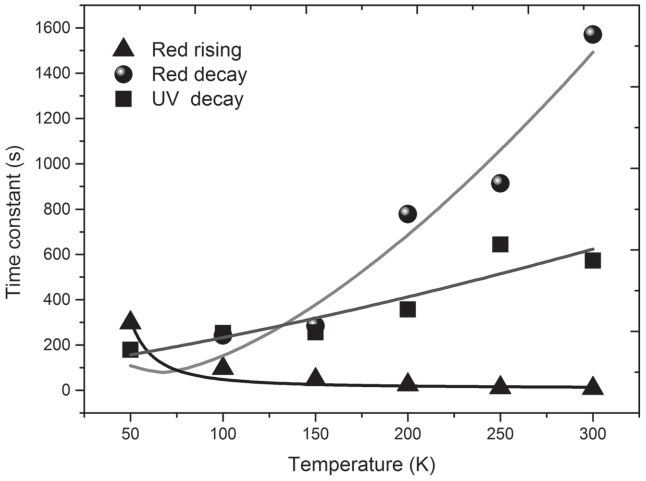

Figure 4. Time constants as a function of temperature for different processes. The time constant was obtained by fitting the current change at the initial stage just after the red/633 nm (UV/365 nm) light is switched on/off. The triangle, sphere and square symbols represent the time constant of the current rising process just after the red light is on, the current decay process just after the red light is off, the current decay process just after the UV light is off, respectively. The solid lines are the fitting results using a different function.

The electrodes (Cr/Au (5/50 nm)) were then patterned with standard photolithography, electron beam metal deposition, and lift-off. Atomic force microscopy (AFM) was used to determine the thickness of BP flake under the AC mode.

Raman Characterization: Raman measurements were performed in a Witec system in backscattering configuration. The excitation was provided by visible laser light (λ = 532 nm) through a 100× objective (NA = 0.95). To avoid laser-induced modification or ablation of the samples, all spectra were recorded at low power levels. For the polarization resolved Raman measurement, the angle between excitation light band the crystal *b*-axis was tuned by rotating the crystal while keeping the excitation light unchanged.

Optoelectronic measurement: All the electronic and optoelectronic characterization were performed in a probe station under vacuum condition, where the temperature can be tuned from room temperature to 50 K. The photocurrent was recorded by the Agilent 1500A semiconductor analyzer under global illumination condition. The light excitation was provided by diode-pumped solid state lasers operated in continuous wave mode with different wavelengths of 405, 532, and 633 nm, respectively. The 365 nm lamp was used for the UV excitation.

Supporting Information

Supporting Information is available from the Wiley Online Library or from the author.

Acknowledgements

The authors acknowledge Yoshinori Okada for fruitful discussion, and Zhangru Xiao and Chuanhong Jin for their assistance on HRTEM characterizations, and the Center of Electron Microscopy of Zhejiang University for the access to microscope facilities. This work is supported by the Singapore National Research Foundation under NRF RF Award No. NRF-RF2013-08, the start-up funding from Nanyang Technological University (M4081137.070). H.J.F acknowledges support by the Ministry of Education of Singapore Tier 3 grant (MOE2011-T3-1-005).

Received: April 29, 2016
Revised: May 23, 2016
Published online: July 4, 2016

[1] Y.-M. Lin, C. Dimitrakopoulos, K. A. Jenkins, D. B. Farmer, H.-Y. Chiu, A. Grill, P. Avouris, *Science* **2010**, *327*, 662.
[2] B. Radisavljevic, A. Radenovic, J. Brivio, V. Giacometti, A. Kis, *Nat. Nanotechnol.* **2011**, *6*, 147.
[3] F. Schwierz, *Nat. Nanotechnol.* **2010**, *5*, 487.
[4] F. Liu, S. Zheng, X. He, A. Chaturvedi, J. He, W. L. Chow, T. R. Mion, X. Wang, J. Zhou, Q. Fu, *Adv. Funct. Mater.* **2016**, *26*, 1169.
[5] F. Xia, T. Mueller, Y.-m. Lin, A. Valdes-Garcia, P. Avouris, *Nat. Nanotechnol.* **2009**, *4*, 839.
[6] Z. Yin, H. Li, H. Li, L. Jiang, Y. Shi, Y. Sun, G. Lu, Q. Zhang, X. Chen, H. Zhang, *ACS Nano* **2011**, *6*, 74.
[7] C. Chen, S. Rosenblatt, K. I. Bolotin, W. Kalb, P. Kim, I. Kymissis, H. L. Stormer, T. F. Heinz, J. Hone, *Nat. Nanotechnol.* **2009**, *4*, 861.
[8] H. Y. Hwang, Y. Iwasa, M. Kawasaki, B. Keimer, N. Nagaosa, Y. Tokura, *Nat. Mater.* **2012**, *11*, 103.
[9] T. Koida, M. Lippmaa, T. Fukumura, K. Itaka, Y. Matsumoto, M. Kawasaki, H. Koinuma, *Phys. Rev. B* **2002**, *66*, 144418.
[10] L. Li, C. Richter, J. Mannhart, R. Ashoori, *Nat. Phys.* **2011**, *7*, 762.
[11] D. Dikin, M. Mehta, C. Bark, C. Folkman, C. Eom, V. Chandrasekhar, *Phys. Rev. Lett.* **2011**, *107*, 056802.
[12] A. Gozar, G. Logvenov, L. F. Kourkoutis, A. Bollinger, L. Giannuzzi, D. Muller, I. Bozovic, *Nature* **2008**, *455*, 782.
[13] A. Ohtomo, H. Hwang, *Nature* **2004**, *427*, 423.
[14] J.-F. Ge, Z.-L. Liu, C. Liu, C.-L. Gao, D. Qian, Q.-K. Xue, Y. Liu, J.-F. Jia, *Nat. Mater.* **2015**, *14*, 285.
[15] W. Rice, P. Ambwani, M. Bombeck, J. Thompson, G. Haugstad, C. Leighton, S. Crooker, *Nat. Mater.* **2014**, *13*, 481.
[16] Y. Lei, Y. Li, Y. Chen, Y. Xie, Y. Chen, S. Wang, J. Wang, B. Shen, N. Pryds, H. Hwang, *Nat. Commun.* **2014**, *5*, 5554.
[17] A. L. Yeats, Y. Pan, A. Richardella, P. J. Mintun, N. Samarth, D. D. Awschalom, *Sci. Adv.* **2015**, *1*, e1500640.
[18] C. R. Dean, A. F. Young, I. Meric, C. Lee, L. Wang, S. Sorgenfrei, K. Watanabe, T. Taniguchi, P. Kim, K. Shepard, *Nat. Nanotechnol.* **2010**, *5*, 722.
[19] L. Britnell, R. Ribeiro, A. Eckmann, R. Jalil, B. Belle, A. Mishchenko, Y.-J. Kim, R. Gorbachev, T. Georgiou, S. Morozov, *Science* **2013**, *340*, 1311.
[20] F. Withers, O. Del Pozo-Zamudio, A. Mishchenko, A. Rooney, A. Gholinia, K. Watanabe, T. Taniguchi, S. Haigh, A. Geim, A. Tartakovskii, *Nat. Mater.* **2015**, *14*, 301.
[21] P. Rivera, J. R. Schaibley, A. M. Jones, J. S. Ross, S. Wu, G. Aivazian, P. Klement, K. Seyler, G. Clark, N. J. Ghimire, *Nat. Commun.* **2015**, *6*, 6242.
[22] X. Hong, J. Kim, S.-F. Shi, Y. Zhang, C. Jin, Y. Sun, S. Tongay, J. Wu, Y. Zhang, F. Wang, *Nat. Nanotechnol.* **2014**, *9*, 682.
[23] M. Massicotte, P. Schmidt, F. Vialla, K. Schädler, A. Reserbat-Plantey, K. Watanabe, T. Taniguchi, K. Tielrooij, F. Koppens, *Nat. Nanotechnol.* **2016**, *11*, 42.
[24] L. Li, Y. Yu, G. J. Ye, Q. Ge, X. Ou, H. Wu, D. Feng, X. H. Chen, Y. Zhang, *Nat. Nanotechnol.* **2014**, *9*, 372.
[25] J. Qiao, X. Kong, Z.-X. Hu, F. Yang, W. Ji, *Nat. Commun.* **2014**, *5*, 4475.
[26] F. Xia, H. Wang, Y. Jia, *Nat. Commun.* **2014**, *5*, 4458.
[27] H. Liu, A. T. Neal, Z. Zhu, Z. Luo, X. Xu, D. Tománek, P. D. Ye, *ACS Nano* **2014**, *8*, 4033.

[28] R. A. Doganov, E. C. O'Farrell, S. P. Koenig, Y. Yeo, A. Ziletti, A. Carvalho, D. K. Campbell, D. F. Coker, K. Watanabe, T. Taniguchi, *Nat. Commun.* **2015**, *6*, 6647.
[29] X. Chen, Y. Wu, Z. Wu, Y. Han, S. Xu, L. Wang, W. Ye, T. Han, Y. He, Y. Cai, *Nat. Commun.* **2015**, *6*, 7315.
[30] V. Tayari, N. Hemsworth, I. Fakih, A. Favron, E. Gaufrès, G. Gervais, R. Martel, T. Szkopek, *Nat. Commun.* **2015**, *6*, 7702.
[31] V. Tran, R. Soklaski, Y. Liang, L. Yang, *Phys. Rev. B* **2014**, *89*, 235319.
[32] J. Pei, X. Gai, J. Yang, X. Wang, Z. Yu, D.-Y. Choi, B. Luther-Davies, Y. Lu, *Nat. Commun.* **2016**, *7*, 10450.
[33] M. Buscema, D. J. Groenendijk, G. A. Steele, H. S. van der Zant, A. Castellanos-Gomez, *Nat. Commun.* **2014**, *5*, 4651.
[34] N. Youngblood, C. Chen, S. J. Koester, M. Li, *Nat. Photonics* **2015**, *9*, 247.
[35] M. Buscema, D. J. Groenendijk, S. I. Blanter, G. A. Steele, H. S. van der Zant, A. Castellanos-Gomez, *Nano Lett.* **2014**, *14*, 3347.
[36] S. Lu, L. Miao, Z. Guo, X. Qi, C. Zhao, H. Zhang, S. Wen, D. Tang, D. Fan, *Opt. Express* **2015**, *23*, 11183.
[37] X. Wang, A. M. Jones, K. L. Seyler, V. Tran, Y. Jia, H. Zhao, H. Wang, L. Yang, X. Xu, F. Xia, *Nat. Nanotechnol.* **2015**, *10*, 517.
[38] H. Yuan, X. Liu, F. Afshinmanesh, W. Li, G. Xu, J. Sun, B. Lian, A. G. Curto, G. Ye, Y. Hikita, *Nat. Nanotechnol.* **2015**, *10*, 707.
[39] Z. Luo, J. Maassen, Y. Deng, Y. Du, R. P. Garrelts, M. S. Lundstrom, D. Y. Peide, X. Xu, *Nat. Commun.* **2015**, *6*, 8572.
[40] Z. Guo, H. Zhang, S. Lu, Z. Wang, S. Tang, J. Shao, Z. Sun, H. Xie, H. Wang, X. F. Yu, *Adv. Funct. Mater.* **2015**, *25*, 6996.
[41] H. B. Ribeiro, M. A. Pimenta, C. J. de Matos, R. L. Moreira, A. S. Rodin, J. D. Zapata, E. A. de Souza, A. H. Castro Neto, *ACS Nano* **2015**, *9*, 4270.
[42] X. Wang, Z. Cheng, K. Xu, H. K. Tsang, J.-B. Xu, *Nat. Photonics* **2013**, *7*, 888.
[43] O. Lopez-Sanchez, D. Lembke, M. Kayci, A. Radenovic, A. Kis, *Nat. Nanotechnol.* **2013**, *8*, 497.
[44] K. Roy, M. Padmanabhan, S. Goswami, T. P. Sai, G. Ramalingam, S. Raghavan, A. Ghosh, *Nat. Nanotechnol.* **2013**, *8*, 826.
[45] M. Huang, M. Wang, C. Chen, Z. Ma, X. Li, J. Han, Y. Wu, *Adv. Mater.* **2016**, *28*, 3481.
[46] H. Yamada, G. Miller, *J. Solid State Chem.* **1973**, *6*, 169.
[47] C. Lee, J. Destry, J. Brebner, *Phys. Rev. B* **1975**, *11*, 2299.